이학석사학위논문

Enhanced drug delivery systems using pH-responsive peptides and reverse electrodialysis

pH-응답성 펩타이드와 역전기투석을 이용한
향상된 약물 전달 시스템

2017년 8월

서울대학교 대학원
화학부 생화학 전공

장 주 명

Enhanced drug delivery systems using pH-responsive peptides and reverse electrodialysis

지도교수 이 연

이 논문을 이학석사학위논문으로 제출함

2017년 8월

서울대학교 대학원

화학부 생화학 전공

장 주 명

장주명의 석사학위논문을 인준함

2017년 8월

위 원 장 **이 형 호 (인)**

부 위 원 장 **이 연 (인)**

위 원 **김 석 희 (인)**

Abstract

Enhanced drug delivery systems using pH-responsive peptides and reverse electrodialysis

장주명 (Joomyung Jang)
Department of Chemistry
College of Natural Sciences
Seoul National University

The purpose of this study was to increase the efficacy and safety of drugs in the biosystem. Two methods have been used in my research.

First study is giving pH-selectivity to LK peptide which is a cell penetrating peptide composed of leucine (L) and lysine (K) with high cell penetrating ability at 10 nM level. I introduced histidine (H) with a pKa of 6.0 in the sequence of the LK peptide to introduce pH-sensitivity into the peptide. As a result, I have developed a new LH peptide which can be protonated at about pH 6 and represent positive charges for the internalization into cells. The LH peptide could be used as an cancer-targeting drug carrier, because the pH around cancerous tissues is about 5-6. I confirmed that the LH peptide selectively penetrates into the cells depending on the pH. Moreover, I compared the toxicity of the LH peptide at different pH conditions.

Secondly, I introduced Reverse Electrodialysis (RED) into transdermal drug delivery system. RED patch could generate the electrical energy

from the ion gradient of two salt solution of different concentrations across ion-selective membranes. I used the generated electrical energy for delivering ionic drugs into skin. I confirmed that the ionic drugs were efficiently delivered by the RED system in *in vitro* penetration test. Finally, through a cooperative research, I examined the in vivo pharmacological effects of risedronate delivered by RED in osteoporosis-induced mouse models.

I believed that both studies will be used as effective alternatives for drug delivery with high efficiency and safety in near future.

Keyword: pH-selectivity, Cell penetrating peptide, Reverse electrodialysis(RED), Transdermal drug delivery, Iontophoresis, Osteoporosis, Risedronate

Student number: 2015-20402

Contents

Introduction

The lifespan of human beings has been increasing with the discovery or development of remedies against fatal diseases in the past. However, development of new drugs has a critical drawback in terms of cost and time. It is estimated that the development of new drugs costs an astronomical sum (about $ 2.6 billion) and it takes more than 10 years for preclinical and clinical procedures(1).

Therefore, studies are being actively carried out to develop drug formulations and devices to deliver drugs that have been previously developed and was proven to be efficient and safe to the body, instead of *de novo* deveopment of new drugs. This process is called as the drug delivery system (DDS), which is considered to have a potential to improve the drug's efficacy by controlling the position, time, and speed of drug release in the body. DDS has the advantages of expanding bioavailability or duration of the drug, minimizing degradation or loss of the drug, and preventing side effects of the drug (2,3).

In this study, I researched pH-selective drug delivery and new type of transdermal drug delivery method for efficient and safe drug delivery. In Part I, I developed a pH-responsive cell penetrating peptide (CPP) by introducing histidines into LK peptide. In Part II, I developed a novel transdermal drug delivery method using reverse electrodialysis (RED). I applied a miniaturized RED patch for efficient delivery of ionic drugs into skin.

Part Ⅰ

1. Introduction

Cell penetrating peptide (CPP) is a short sequence peptide capable of penetrating the cell membrane and entering into the cells (4). Currently, how CPPs could penetrate into the cell is not known precisely. It has been suggested that CPPs penetrate cellular membrane through endocytosis, direct penetration, or both at the same time (4, 5, 6). Cell-penetrating peptides can be classified according to their production methods, including protein-derived peptides obtained by protein expression through cells, chimeric peptides formed by binding two proteins or peptides, and synthetic peptides synthesized through amide bonds by one amino acid (4). CPPs is also classified by structure: a polycationic peptide composed of only cationic amino acids and an amphipathic peptide composed of hydrophobic amino acids and hydrophilic amino acids. CPPs have been used as a useful carrier for drug delivery because it exhibits low toxicity while penetrating cells at a relatively low concentration (4, 6).

In the previous studies, LK peptides which have cell penetrating ability at 10 nM level have been developed by making a dimer of an α-helical peptide composed of leucine (Leu, L) and lysine (Lys, K) (7). However, such peptides have a problem that LK dimer does not selectively enter to specific cells or tissues. In order to solve this problem, the present study aimed to give selectivity to LK peptide, and pH was selected as a means to give selectivity. In general, the periphery of normal cells maintains a pH of about 7.4, but in the case of cancer cells, the pH is lower than the condition of normal cells (pH 5-6) (8, 9). Then, I anticipated that modified LK peptide could penetrate into cancer cells selectively at low concentration level. In order to increase pH-selectivity of CPPs at

the surrounding pH of cancer cells, histidine (His, H) was introduced instead of Lys of LK peptide, and cell penetrating ability was confirmed through *in vitro* experiments (10, 11). I also investigated the relationship between structure and cellular uptake of modified peptide (LH peptide). Finally, I checked the cytotoxicity of LH peptide.

2. Materials and methods

2.1 Materials

N-α-Fmoc protected L-amino acids, Rink Amide MBHA resin (0.6-0.9 mmol/g loading), and benzotriazole-1-yl-oxy-tris-pyrrolidino-phosphonium hexafluorophosphate (PYBOP) were purchased from Beadtech (Ansan, Gyeonggi, Korea). Dimethylformamide (DMF), 1, 2-dichloromethane (DCM), trifluoroacetic acid (TFA), triisopropylsilane (TIS), piperidine, 5(6)-carboxytetramethylrhodamine were purchased from Sigma-Aldrich (St. Louis, MO, USA). N, N-diisopropylethylamine (DIPEA), N, N'-1, 4-phenyl-enedimaleimide and 1, 2-ethanedithiol (EDT) were purchased from TCI (Japan). N-hexane and diethyl ether were purchased from SAMCHUN chemical (Pyeongtaek, Gyeonggi, Korea).

2.2 Synthesis of LH peptides

Synthesis of LH2 (sequence: LHHLCHLLHHLCHLAG) was performed by using an Fmoc-based solid-phase peptide synthesis with Rink Amide MBHA resin. First of all, Rink Amide MBHA resins (100 mg, 0.6-0.9 mmol/g loading) were deprotected with 20% piperidine in DMF (2 mL), and then Fmoc protected first amino acid, glycine (160.55 mg, 0.54 mmol), Benzotriazole-1-yloxy-tris-pyrrolidino-phosphonium hexafluorophosphate (PyBOP) (281.01 mg, 0.54 mmol), and N,N-diisopropylethylamine (DIPEA) (92 μL, 0.54 mmol) were stirred at room temperature for 3h. The by-products of reaction were removed with DMF solvents (3 mL × 5 times). After coupling step, Fmoc-protected first amino acid was de-protected with 20% piperidine in DMF, and the byproducts of reaction were removed with DMF solvents (3 mL × 5 times). The coupling and deprotection steps were repeated with different Fmoc-protected amino

acids sequentially until deprotection of the last Fmoc-protected amino acids. The deprotected resin-bound peptide was washed with DMF and DCM solvents to remove piperidine. The N-terminus of this peptide was then acetylated by adding a solution of acetic anhydride (1.35 mmol, 127.4 μL) and N-hydroxybenzotriazole (HOBt) (1.35 mmol, 182.4 mg) in a solvent (DMF:DCM) (2 mL, v/v= 90:10). The reaction mixtures were stirred for 2 h at room temperature. Cleavage of all peptides from solid support was carried out by treatment with a cleavage mixture consisting of TFA/TIS/EDT/water (2 mL, v/v=94:1:2.5:2.5) for 2 h at room temperature. The cleaved resin was then separated by filtration and further washed with TFA (3 mL). The separated peptide solution was concentrated by blowing nitrogen gas. The synthesized peptides were precipitated with n-hexane and diethyl ether mixture at the equal volume (v/v = 50:50). After the resulting suspension was centrifuged at 3,500 rpm for 5 min at room temperature, the supernatant was carefully discarded. These processes are repeated three times. Then, the pellet was left under high vacuum condition for 12h. All peptides were purified with HPLC (Shimadzu Prominence series) with a Zorbax C-18 (5 μm, 9.4 x 250 mm) column. For the mobile phase, Solution A (distilled water with 0.1% v/v TFA) and Solution B (acetonitrile with 0.1% v/v TFA) were used as eluent solutions. LH peptide was eluted at 30-70% of Solution B. Mass Spectra of peptides were obtained using a MALDI-TOF mass instrument MS (M+H+): 1893.7 (calcd.), 1895.0 (found). The HPLC chromatogram of LH2 is shown (>95% purity) (Fig. 2).

2.3 Dimerization of LH peptide

Dimerization of LH2 was performed under air oxidation for formation of

two disulfide bond between sulfide residues of cysteines. For the synthesis of LH3, purified N-terminal acetylated monomer was dissolved in 0.1 M deaerated ammonium bicarbonate and DMSO (1:1, v/v) up to 4mg/ml concentration. The reaction mixture was stirred open to atmosphere for 24 h.

2.4 Cell culture

MDA-MB-231 cells used in this study were obtained from Korean Cell Line Bank. Cells were maintained with Dulbecco's modified Eagle's medium (DMEM, WelGENE, Gyeongsan, Kyeongsangbuk-do, Korea) containing 10% % fetal bovine serum (WelGENE, Gyeongsan, Kyeongsangbuk-do, Korea). All cell lines were cultured in 5% CO_2 humidified atmosphere at 37℃.

2.5 *In vitro* cellular uptake assay

Quantitative cellular uptake assay

To assess whether LH peptides exhibited better pH-sensitivity than LK peptides, MDA-MB-231 cells (1×10^5cells/well) were plated into 24 well-microplates and cultured for 24h. After four hour long incubation with 2% FBS medium which contained rhodamine labeled peptides and was adjusted to pH 7.4, 7.0, 6.5 or 6.0 respectively, the cells were washed twice with PBS and then incubated with trypsin (20μL/well) for three minuetes. The cells were harvested and centrifuged at 1,000 rpm for 5 min. Subsequently, the cell pellet was suspended and washed once with medium containing 2% FBS and was resuspended in medium containing 2% FBS. Finally, fluorescence intensity of 10,000 cells was analyzed with

an FACS caliber flow cytometer using 488-nm laser excitation.

Confocal laser scanning microscopy (CLSM) observation

MDA-MB-231 cells (5,000 cells/well) were cultured in 180 μL of DMEM with 10% FBS on 35-mm adhesive confocal dish (SPL Lifesciences, South Korea) at 37°C in a humidified 5% CO_2 incubator. After 24 hours, 180 μL of fresh DMEM containing 2% FBS and rhodamine-labeled LH3 was added to the dish and incubated for another 16 hours (final concentration : 25nM). Nuclei were stained with Hoechst 33342 solution (4 μM) for 30 min prior to the microscopy imaging. Cells were washed three times with PBS for the removal of peptides outside the cells, and fresh DMEM with 2% FBS was added. CLSM images were acquired using a Zeiss DE/LSM 510 NLO (Carl Zeiss, Germany) with 500× objective (C-Apochromat, Carl Zeiss). Excitation wavelengths were 545 nm, 450 nm and 633 nm for rhodamine, Lysotracker and Hoechst, respectively.

2.6 Circular dichroism (CD)

Measurements of CD spectra were performed using a Chirascan CD spectrometer (Applied Photophysics) with 1.0 mm path-length cell. CD was scanned from 195 to 260 nm, with integration of 0.25 and bandwidth of 1 nm. The average was obtained through three iterations. LH and LK peptides were measured in 10mM phosphate buffer. Then I controlled the pH of PBS used to dissolve peptides (pH 7.4, 6.5, 6.3, 6.0, and 5.8)

2.6 *In vitro* cytotoxicity assay

CCK assay

Cytotoxicity of all peptides against MDA-MB-231 cells was evaluated using

the CCK assay under various pH conditions (pH 7.4, 7.0, 6.5 and 6.0). Cells were seeded at 1 × 10^4cells/well in 96-well plates, 24h before treatment. After washing, cells were treated with medium containing 2% FBS and was adjusted to pH 7.4, 7.0, 6.5 or 6.0, and containing various concentrations of peptides. After 4 h incubation, 10 μL of CCK (5 mg/mL) was added to each well and incubated for another 1 hour at 37°C. Then, the absorbance was determined using a microplate reader at 450 nm. Cell viability (%) was calculated using the following equation: $A_{test} / A_{control} \times 100\%$, where A_{test} and $A_{control}$ represent the absorbance of cells treated with different test solutions and blank culture media, respectively.

3.Results

3.1 Cellular uptake assay of LH peptides

I measured cell penetrating ability of monomers and dimers of rhodamine-labeled LH peptide using MDA-MB-231 cells through flow cytometry analysis (FACS). Monomers and dimers of rhodamine-labeled LK peptides were used as reference materials for comparison. LK monomer (LK2) showed slightly increased cellular uptake at pH 7.0 but cellular uptake decreased as pH dropped to 6.5 and 6.0. (Fig. 3A). In contrast, the LH monomer (LH2) showed increased cell penetrating ability with decreasing pH. Comparing the dimer of LH (LH3) with the dimer of LK (LK3), the LK dimer shows a slight increase in cellular uptake at pH 7.0 and it decreases with decreasing pH to 6.5 and 6.0, while cellular uptake of LH dimer is higher at pH 7.0 and 6.5 (Fig. 3B). However, cellular uptake of LH dimer decreased at pH 6.0.

Then, confocal laser scanning microscopy was used to monitor the uptake and localization of LH3 in cells. Rhodamine-labeled LH3 showed red color and nuclei and lysosomes were stained blue and green, respectively. LH3 showed similar cell uptake at pH 7.4, 7.0 and 6.5, and cellular uptake of LH3 at pH 6.0 seems to increase significantly.

3.2 Structural characterization of LH peptides using CD

I investigated the secondary structure and pH-dependent conformational transition of LH and LK peptides by circular dichroism (CD) spectroscopy. Cells were treated with peptides in five different pH conditions (pH 7.4, 6.5, 6.3, 6.0, and 5.8) for a more detailed comparison. As pH decreases,

ellipticity values in CD spectra of LH2 at 208 and 222 nm were lower and value at 193 nm was higher except for those values at pH 5.8 (Fig. 5A). At pH 6.0 condition, I could confirm the ellipticity value at 208 and 222 nm was the lowest and the ellipticity value at 193nm was the highest among values at five different pH conditions. Interestingly, the ellipticity value of LH2 at pH 5.8 was similar with the value at pH 7.4. Even the minimum ellipticity value at 220 nm in pH 5.8 was higher than that in pH 7.4. In the case of LK2, a similar aspect of spectra was obtained in pH 7.4, 6.5 and 6.3. However, the ellipticity value in pH 6.0 and 5.8 was low at 210 nm or less, and the value was close to zero at 190 nm.

3.2 Cytotoxicity test

I examined the cytotoxicity of the LH peptide by varying the pH. LH dimer When LH dimer (LH3) was treated only, it was not toxic up to 1μM regardless of pH (Fig. 6). When treated with MTX only, the survival rate was 40-60% at 1 μM concentration although it showed slight difference upon varied pH.

4. Discussion

It is estimated that positively charged amino acid residues (lysine, arginine etc.) are necessary to bind and enter cells. However, positively charged residues are accountable for non-specific cellular uptake. In this study, I developed pH-selective CPP introducing histidines into the position of lysines on LK peptide sequence. Histidine is protonated and positively charged below pH 6.0 because an imidazole side chain in histidine has a pKa of around 6.0 (Fig 1B). LK peptide which has cell penetrating ability at 10nM level has been reported. Six lysines in LK peptide (LKKLCKLLKKLCKLAG) were substituted with histidines (LHHLCHLLHHLCHLAG) (Fig. 1A).

From the cellular uptake assay, the penetration of LK2 showed little increase as the pH decreased from 7.4 to 7.0. Then, the penetration of LK2 decreased as the pH decreased from 7.0 to 6.5, and 6.0 (Fig. 3A). Especially, LK2 showed about 20% of cell penetrating ability at pH 6.0 which is almost half of the penetrating ability at pH 7.4. On the other hand, LH2 showed similar penetrating ability at pH 7.4 and 7.0 (Fig. 3B). As pH decreased from 7.0 to 6.5, and 6.0, cellular uptake increased gradually. As a result, the penetrating ability of LK2 decreased to almost half when the pH was changed to 6.0, but the penetrating ability of LH2 increased by about 30% when the pH was changed to 6.0. The penetrating ability of LK3 showed little difference at pH 7.4, 7.0, and 6.5, and slightly lower cellular uptake at pH 6.0, while the penetrating ability of LH3 increased about 30% from pH 7.4 to pH 7.0 and 6.5. and slightly decreased at pH 6.0.

I could also confirm enhanced cell penetrating ability of LH3 with lower pH condition through CLSM images. However, when compared with the

FACS results, the tendency of cell penetrating ability was different with respect to change in pH conditions. From the results of CLSM, LH3 showed the highest cell permeability at pH 6.0.

When comparing the spectra of CD on LK2 and LH2, in case of LH2, similar spectra were obtained at three pH conditions (pH 6.0, 6.3 and 6.5) except for pH 5.8 and 7.4 (Fig. 5A). The ellipticity values of LH2 had negative band at 222 nm and 208 nm, a positive band at 193 nm, which represented that LH2 forms α-helical secondary structure from pH 6.0 to pH 6.5. Even at pH 7.4 and pH 5.8, LH2 appears to form an alpha helical structure, but it appears to have a loosened helix compared to the peptides in previous three pH conditions. Although it was not significantly different among three conditions, LH2 formed the most predominant alpha-helical structure at pH 6.0. Associating this with FACS results, I found that, LH peptides also have a significant effect on alpha-helicity. This corresponds to previous studies suggesting that LK peptides with more α-helical structure can penetrate into the cells (7) (Fig. 5A and 3A). Then, I confirmed that α-helicity of LK2 decreased with lower pH conditions (pH 5.8 and 6.0) (Fig. 5A). The cell penetrating ability and α-helicity of LK2 decreased with lowering the pH conditions (Fig. 5A and 3B). This results also showed the relationship between the cellular uptake and α-helicity (7).

From the cell cytotoxicity assay, I confirmed that LH3 itself showed almost no toxicity to cells as survival rate is more than 90% regardless of pH up to 1 μM level (Fig. 6).

5. Summary

In this study, I developed pH-selective CPP, LH peptide, by introducing histidines into the position of lysines in LK peptide. LH peptide would be positively charged at pH 6.0 condition, which is similar to around cancer cells, because the pKa of histidine is about 6.0. Then, I confirmed that LH monomer and dimer could penetrate into cells selectively at pH 6.0, and 6.5 compared to 7.4. Cell penetrating ability of LH3 showd 30 % increase as pH decreased from 7.4 to 6.5 (60% → 90%) while that of LK3 showed almost no difference (70%) according to pH change.

I also confirmed the cell penetrating ability with the change of pH conditions. Althogh the pH condition showing the highest cellular uptake was different between results of FACS and CLSM, I could know that cell penetrating ability of LH3 is maximum at the range from pH 6.0 to 6.5. LH2 had higher cell permeability and α-helicity with lowering the pH conditions, and showed the highest cellular uptake at pH 6.0.

Then, I checked cytotoxicity of LH3. LH3 was found to be nearly non-toxic up to 1 concentration.

LH peptide showed selectively cellular uptake at about pH 6 similar to the surrounding cancer cells. As pH decreases, α-helicity of LH peptides increases then, cell penetrating ability could become enhanced. pH-selective LH peptides are expected to be potent alternative as an anticancer drug carrier.

Part Ⅱ

1. Introduction

The transdermal drug delivery system refers to a method of delivering a drug through the skin instead of oral administration or injection administration. In contrast to oral administration, it is possible to avoid the first-pass metabolism of the drug that may occur in the liver and the inactivation of the drug by digestive enzymes or digestive fluids in the stomach by using transdermal drug delivery system (12, 13). It is also a good alternative to patients who have allergic reactions such as irritation or rash on needles. Then, transdermal drug delivery doesn't induce pain as compared to injections, and it has higher patient acceptance because it can be administered by the patients themselves. For these advantages, many studies of this field have actively been conducted.

The challenge of transdermal drug delivery system is penetrating drugs through the stratum corneum which exists at the outermost of the skin (14). The stratum corneum has a 'brick & mortar' model of corneocytes coated with lipid bilayer and an extracellular matrix consisted of lipid layer-structure (15). For these reasons, it is difficult for the hydrophilic drug to penetrate the skin. Then, several methods were developed to overcome this challenge (16, 17). One of them is 'iontophoresis' which is a method of delivering drugs into the skin through electrical energy (18). This method can deliver ionic drugs through flowing current from the power supply to the electrodes.

Studies on iontophoresis have been actively carried out, and various products are being commercialized in the market. However, when using commercial iontophoretic devices, valuable metals such as Pt or Ag are

mainly used as an electrode (19). When such a metal electrode is used, water electrolysis reaction occurs in the electrode attached to the skin. Then a proton is generated on the skin and this causes pH-change resulting in skin irritation (20, 21). In addition, the proton or chloride ion generated from the electrode more easily penetrates into skin than the drugs because of the much smaller molecular weight. These fast transfers of ions may interrupt efficient delivery of ionic drugs. These devices also have disadvantage in that they are inconvenient to carry. They are composed of three parts (power supply, patch, and electrode). To overcome these drawbacks, I created a portable small patch using reverse electrodialysis to generate current, without using electrodes to avoid possible skin damage.

Reverse electrodialysis (RED) is a method in which cation exchange membranes (CEM) and anion exchange membranes (AEM) are sequentially stacked, and high- and low concentrated NaCl solutions are alternately filled between the membranes. When the solution is filled, Na+ andCl- ions move through the opposite membrane, which generate the electrical energy. I miniaturized the technique into a patch form, and the drug was stored in the hydrogel instead of the electrode at the bottom of the patch attached to the skin (Fig. 11). Thereby, the electrical energy can be produced without using the power source, and a portable patch can be made without using the electrode.

In this experiment, three ionic drugs (lidocaine, ketorolac, risedronate) were delivered through *in vitro* drug delivery experiment. I also investigated the pharmacological effects of risedronate in osteoporosis - induced mouse models through *in vivo* experiments. This small RED patch is expected to be a promising alternative to transdermal drug delivery in the future.

2. Materials and methods

2.1. Materials

Ketorolac tromethamine (KT), lidocaine hydrochloride (LID), risedronate monosodium (RIS), sodium chloride, acrylamide, N,N'-methylenebisacrylamide, and 2,2'-azobis(2-methylpropionamidine) dihydrochloride were bought from Sigma-Aldrich (St. Louis, MO, USA). The 22 G sterile hypodermic needle were purchased from Kovax-Syringe; Korea vaccine co., Ltd., South Korea. Selemion CMV and AMV were bought from Asashi Glass Co., Ltd. Double-faced waterproofing tape was ordered from ACE cross SBX, Japan. High pressure liquid chromatography (HPLC)-grade solvents were obtained from J.T. Baker (Mallinckrodt Baker, Inc., Phillipsburg, NJ). Distilled water (Barnstead Nano-pure Diamond, 18.2 MW/cm of resistance) was used in all experiments.

2.2. Fabrication of reverse electrodialysis (RED) patch

Fig. 8 and 9 show schematic figure of 10 IEM-paired RED patch. An IEM pair in the RED is composed of a cation exchange membrane (CEM) and an anion exchange membrane (AEM), and a spacer between two layers of the double-faced waterproofing tape. The double-faced waterproofing tape (thickness: 250 mm/layer, length: 2.0 cm, width: 4.0 cm) has two square holes (1.0 × 1.0 cm^2) between the membranes. The hypodermic needles were placed in every hole between two membranes for the injection of NaCl solutions. After 10 IEM pairs were stacked alternatively, 3-layered double-faced waterproofing tape with a rectangular hole inside (3.0 × 1.0 cm^2) and 3-layered long spacer (3.0 × 1.0 cm^2) were attached onto the uppermost floor. Finally, the top of the RED

patch was covered with a projector film (4.0 × 2.0 cm^2). In the lowest floor, two layers of double-faced waterproofing tape were added for hydrogels storing drugs. For the activation of the RED patch, every hole was filled with NaCl solutions (4.4M and 0.011M concentration) through the needles in alternative pattern. 4.4M NaCl solution was injected into the uppermost space for high conductivity.

2.3. Preparation of hydrogels

A hydrogel of RED patch is used as a drug reservoir attached onto the skin. The polyacrylamide hydrogel (30% w/v) was prepared from a solution consisted of acrylamide (monomer), N,N'-methylenebisacrylamide (cross-linker) and 2,2'-azobis(2-methylpropionamidine) dihydrochloride (initiator) in distilled water. Finally, drugs were added in the solution just before the polymerization. NaCl, the counterpart of the drug-containing hydrogel, was added to the monomer solution to make the final NaCl concentration of 50 mM. The monomer solution (150μL) was placed on a glass mold (1.0 × 1.0 cm^2) and heated at 100°C for 3 minutes for polymerization. The polymerized hydrogel was cooled and placed to the lowest IEM of the RED patch. For positively charged drugs, the hydrogel with drugs was placed on the AEM and for negatively charged drugs, the hydrogel with drugs was placed on the CEM side (Fig. 8). Hydrogels without drugs were placed on the opposite site of hydrogels containing drugs.

2.4. Quantitative measurement of drugs

Three drugs (RIS, KT, and LID) were analyzed by HPLC (Model 1200, Agilent, USA) (18-20). Detection wavelengths were 262, 230, and 230 nm for quantitative analysis of RIS, KT, and LID, respectively. All chromato-

graphic separation was conducted with a C18 column (Agilent symmetry C18, 150 mm × 4.6 mm, 5 μm) at a flow rate of 1 mL/min and an injection volume of 25 μL. The mobile phase for RIS analysis was a mixture (7:93) of acetonitrile and an aqueous solution (pH 7.0) of sodium pyrophosphate (5 mM) and tetra-n-butyl ammonium hydrogen bromide (5 mM). The mobile phase was a mixture (25:75) of acetonitrile and ammonium acetate buffer (0.1 M, pH 4.0) for KT. The mobile phase was a mixture (40:60) of methanol and an aqueous solution of sodium dihydrogen phosphate (0.1 M) and tetra-n-butyl ammonium hydroxide (5 mM) for LID.

2.5. *In vitro* penetration test through skin

Eight-week old C57BL/6 mice were bought from Orient Bio, Inc. (South Korea) and used for the *in vitro* penetration test (female for RIS / male for KT and LID). Whole *in vitro* penetration tests were approved by the Institutional Animal Care and Use Committees of Seoul National University (SNU-151228-6). The mice were sacrificed and full-thickness skin samples were cut off just before injection of NaCl solution into RED patch. Obtaining the skin samples was officially permitted by the animal care committee of Seoul National University. The subcutaneous fat and capillary vessels were torn off from the skin samples carefully. The skin samples were wiped with gauze soaked with phosphate buffered saline (PBS, pH 7.4) slightly, and then the bottom side of the sample was placed on the self-manufactured Franz-diffusion cell (area : 1.5 x 3.5 cm^2, volume : 7mL) (Fig. 10). Both hydrogels with and without drugs (drugs and 50mM NaCl) were attached to the skin sample. PBS solution (pH7.4) was used as the medium in the chamber part. Digital multimeters

(DMMs) were connected to the RED patch to monitor the electrical currents in real-time (Fig. 11). For the penetration test, the receptor medium was kept under 37℃ and stirred at 200rpm with a magnetic stirring bar for 2 hours. To examine the accumulated RIS with respect to time, every 3.0mL of receptor medium was drawn from the receptor chamber at each time point (15, 30, 45, 60, 90, and 120 min) and drawn volume was filled with the new PBS. After the penetration test (2 hours), the RED patches were isolated from the skin. The voltage of hydrogels attatched to RED patch was measured before and after the penetration test by using a DMM. The amount of drugs left in the skin was extracted by soaking and shaking with PBS solution (pH 7.4) for 48 hours. The amount of drugs from samples was quantified by HPLC.

2.6. *In vivo* therapeutic effects test using ovariectomized mice

10-week-old female C57BL/6N mice were bought from KOATECH (South Korea). All *in vivo* mouse model tests were permitted by the Institutional Animal Care and Use Committees of Kyungpook National University (KNU 2016-0019). Female mice were maintained under the cycles composed of 12-h light term and 12-h darkness term at 22−25℃ in specific pathogen-free (SPF) conditions and with standard rodent chow and water. The mice were ovariectomized (OVX) for induction of osteoporosis (21). Some mice were prepared as SHAM control by a sham surgery. After 4 d, the hair on lateral side (2.5 × 4.5 cm^2) of the mice was removed carefully with an electric shaver.

For *in vivo* experiments, four types of patches were produced depending on the drug content and RED presence: 0.02% RIS in hydrogels (30

μg/mouse) without the RED patch ($GEL_{0.02}$), 0.002% RIS in hydrogels (3 μg/mouse) without the RED patch ($GEL_{0.002}$), 0.02% RIS in the hydrogel with the RED patch ($RED_{0.02}$), and 0.002% RIS in the hydrogel with the RED patch ($RED_{0.002}$). Ovariectomized mice were classified into five groups : OVX, $GEL_{0.02}$, $RED_{0.02}$ $GEL_{0.002}$, and $RED_{0.002}$. Every mice group contained seven to eight mice.

The RED patch was attached to lateral side which was shaved previously on the mouse. The RED patch was kept attached to the mouse for 1 hour under anesthetics. Administration with RED patch was conducted in every 10 days, 3 times in total. Hydrogels without containing RIS were administered to the SHAM and OVX group. After 10 days from the last administration, all groups of mice were sacrificed to extract femora and vertebrae for precise analysis.

2.7. Micro-computated tomography (Micro-CT) analysis

The fourth vertebrae and femur of all mice were scanned with a Quantum FX micro CT (PerkinElmer, USA) to find three dimensional structures. The instrument set ; isotropic voxel size : 10 μm / tube voltage : 90 kVp / tube current : 160 mA / field of view : 5 mm / scan time : 3 minutes. Analyzed 12.0 software was used to calculated morphometric parameters.

Nomenclatures for Bone and Mineral Research follow the instructions of the American Society.

2.8. Statistical analysis

All of the quantitative analysis were replicated at least three times. The data were expressed as mean values ± standard error of the mean

(S.E.M.). The two-tailed Student's t test and one-way analysis of variance (ANOVA) with Bonferroni's test were used to determine statistical significance of the *in vitro* test and *in vivo* experimental results via the GraphPad Prism 5.0 software, respectively. If the p-value was less than 0.05, it was accepted as a significant difference.

3. Results

3.1. *In vitro* penetration of KT and LID using the RED patch

I chosed Ketorolac tromethamine (KT) and lidocaine (LID) as model drugs for cationic and anionic, respectively. I compared the penetrated amount of drugs using the RED patch to the gel only patch (GEL). I used 2% (w/v) drug loaded gel in the patch first, and measured the amount penetrated per area of the skin after administration (2 hours). The amount of KT that penetrated through the skin was only 20.6 ± 7.3 $\mu g/cm^2$ in the GEL group (Fig. 13A). Meanwhile, the amount of KT that penetrated through the skin was 408.3 ± 75.1 $\mu g/cm^2$ in the RED group. There was a 20-fold difference between GEL group and RED group. The amount of KT left in skin was also compared. The residual amount of KT in skin was 25.06 ± 1.50 $\mu g/cm^2$ in GEL group. On the other hand, the residual amount of KT in skin was 61.06 ± 7.28 $\mu g/cm^2$ in the RED group (Fig. 13B). There was a 2.4-fold difference between the GEL group and RED group. In case of LID, the amount of KT that penetrated through the skin was 16.20 ± 7.69 $\mu g/cm^2$ in GEL group. Meanwhile, the amount of KT that penetrated through the skin was 148.9 ± 28.7 $\mu g/cm^2$ in GEL group (Fig. 13C). There was a 9-fold difference between the GEL group and RED group. The amount of LID in the skin was slightly higher in the RED group than GEL group but there was no meaningful difference.

3.2. *In vitro* penetration of RIS

in vitro penetration test of RIS, an anionic drug used for the treat-

ment of osteoporosis, was conducted. Like previous two drugs, hydrogel stored 2% (w/v) RIS. The amount of RIS delivered through RED after 2 hour administration was 420.6 ± 98.0 μg/cm^2 (RED), 36 times higher than the amount of RIS delivered through simple diffusion, 11.67 ± 6.03 μg/cm^2 (GEL) (Fig. 14A). The amount of RIS remaining in the skin in the RED group was 33.18 ± 7.15 μg / cm^2, 2.2times greater than the GEL group of 14.78 ± 3.21 μg/cm^2(Fig. 15).

I also measured the current value of the RED patch over time during the *in vitro* penetration test. The initial current decreased sharply at about 1.2 mA and was almost negligible within 1 hour (Fig. 14B). At the point after 1 hour, the cumulative amount of RIS penetrated through the skin was 358.2 ± 73.9 μg/cm^2 for 1 hour and reached about 85% of the total penetrated amount for 2hours (Fig. 14A). The results present that the amount of RIS penetrated is closely related to the amount of current flowing at that point. Interestingly, the current is reversed after one hour of administration, indicating a negative value (Fig. 14B).

It was also confirmed that when the low concentration of 0.2% (w/v) drug was delivered using RED, the drug penetrated through the skin was increased (Fig. 16). The amount penetrated through the skin at 2 hours after the drug administration was 36.3 ± 6.98 μg / cm^2 in the RED group and 2.37 ± 0.73 μg/cm^2 in the GEL group, and the difference was 15.3 times. In the experiment using 0.2% (w/v), the amount of RIS remaining in the skin was lower than the detection limit in both groups.

I examined how changing the number of IEMs in the RED patch affects the amount of penetrated RIS (Table 2). The amount of RIS penetrated using the RED patch (RED_{6p}) with six pairs of IEM was about half (204. 0± 4.3μg/cm^2) compared to the RED patch (RED) with ten pairs of IEMs (Fig. 17A). The initial current of RED_{6p} started at 500μA

and soon reached a peak at 700μA and then slowly decreased. The graph of current over time for RED_{6p} was almost similar to the aspect of RED and was about half the value compared to RED (Fig. 14B and 15B). Interestingly, the initial voltage of RED_{16p} is 1.5times of initial voltages of RED, but the amount of RIS that penetrated through the skin for $RED1_{6p}$ (Fig 15A and 15C). The change of current for RED_{16p} over time was also not significantly different from RED (Fig. 14B and 15C).

3.3. *In vivo* therapeutic effect of RIS using RED in the osteoporosis-induced mouse model

I have identified *in vivo* pharmacological effect of RIS delivered by RED patch using osteoporosis mouse models induced by estrogen deficiency. RIS was prepared at concentrations of 0.002% and 0.02% in hydrogel, and was administered through mouse skin by simple diffusion (GEL group) and RED patch (RED group). After 30 days from the first dose, spinal bones were harvested by sacrifice of the mice and analyzed by μ CT. Bone Mineral Density (BMD), Bone Volume / Total Volume (BV/ TV), Bone Surface / Bone Volume (BS/BV), Trabecular Separation (Tb.Sp), Trabecular Number (Tb.N) and Trabecular Thickness (Tb.Th) were analyzed to quantitatively compare the pharmacological effects of RIS (Fig. 18A-E). In comparison to the SHAM group, all parameters of the ovaritecomized (OVX) group showed 16% decrease in BMD, 20% decrease in BV/TV, 20% increase in BS/BV, 11% decrease in Tb.Th, 8% increase in Tb.Sp, and 3% decrease in Tb.N. I checked successful formation of osteoporosis induced mouse model by the removal of ovaries. Compared to the OVX group, the $RED_{0.02}$ group showed 37% increase in BMD, 48% increase in BV/TV, 18% decrease in BS/BV, 23% decrease in Tb.Sp, and 20%

increase in Tb.N. Al lmeasured parameters showed substantial differences except the Tb.Th value. In comparison to $GEL_{0.02}$ group, the $RED_{0.02}$ showed 47% increase in BV/TV, 16 % decrease in BS/BV, 21% increase in Tb.N, and 24% decrease in Tb.Sp. The $RED_{0.002}$ with a lower dose of RIS showed no significant change of all parameters except slight increase of BMD. However, GEL groups showed almost no effect on these parameters irrespective of concentrations of RIS.

4. Discussion

I first devised a new patch-type miniaturized RED. The RED device can generate systematically controlled power according to the salt gradient, configuration, and number of IEM pairs. As salt gradient of two different concentrated solutions decreased, the electric potential gradually decreased since the flow of ions decreased. (Fig. 12A).

While the electrical power density of the RED is too low to be considered as an alternative to current existing power supplies, the characteristics of the RED system are very attractive to biomedical applications that require a clinically safe and efficient source of electrical energy. In this regard, this study proposes a promising alternative for a new transdermal drug delivery system based on a miniaturized disposable RED patch.

Because it is difficult to penetrate the skin through simple diffusion, three ionic drugs have been used to determine the feasibility of transdermal drug delivery systems using RED patch (22). KT and RIS, which have negative charge in pH condition of the skin (pH 4-5), and LID with positive charge were selected as model drugs. KT is a potent non-steroidal anti-inflammatory analgesic and can be administered into the body via oral, injection, and transmucosal methods (23). LID is a local anesthetic that can be administered by oral, topical, or injection methods (24). RIS is widely used for clinical treatment of bone disease such as osteoporosis to inhibit activation of osteoclast. In the case of RIS, oral administration is commonly used as a delivery method. Non-invasive transdermal delivery of these drugs is expected to overcome a variety of problems from other methods of administration, like low bioavailability and low specificity. Especially, RIS has a bioavailability of less than

0.5% and also results in severe side effects, like abdominal pain, joint pain and bone necrosis, by oral administration (25). The electrical power generated by the salt gradients could efficiently enhance penetration of all ionic drugs.

In the *in vitro* penetration study of KT and LID, the penetrated amount of RED group was significantly increased 9 times in LID and 20 times in KT respectively, against the GEL group (Fig. 13). The residual amount of drug in the skin was similar to the amount penetrated through the skin In the GEL group, whereas the amount of penetrated drugs was 6-12 times higher than the residual amount of drug in the skin in the RED group. This result clearly shows that RED improves the delivery of ionic drugs into the skin regardless of the charge state of a drug.

RIS has both positive and negative charge with a net negative charge of -1 or -2 at the skin pH due to the pKa value of 1.6, 2.2, 5.9, 7.1 and 11.7 (26). Therefore, transdermal delivery through the simple diffusion was very hindered due to the high hydrophilicity of RIS (Fig. 14A). However, when using RED, the relative penetration of RIS was the highest among the three model drugs with similar molecular weights (about 36-fold increase). The high charge density of RIS is expected to have an impact on delivery efficiency compared to the other two drugs.

The effect of transdermal drug delivery via RED is influenced by the amount of drug stored in the hydrogel and the initial voltage. The penetrated amount of 0.2% drug, which is ten times smaller than the basic type of 2%, decreased (Fig. 16). Furthermore, RED (10-IEM-paired) showed about two times higher initial voltage than RED_{6p} (6-IEM-paired), and the amount of delivered drugs through RED was also about two times higher than RED_{6p} (Fig. 17). In contrast, when the RED and RED_{16p} (16-IEM-paired) were compared, the initial voltage of RED_{16p} was about

1.5 times higher than initial voltage of the RED, but the amount of RIS penetrated was not significantly different. This phenomenon is thought to be due to the concentration gradient in the hydrogel, which causes the current to saturate (Fig. 17).

In the graph of current over time, the maximum current of 1.2 mA and the current reversal over 1 hour are shown in both RED and RED_{16p} and RED_{6p} also showed similar aspect except for the figures of Y-axis (Fig. 14B, 15B and 15C). It can be seen that the life time of the RED as an electrical source is about one hour. In addition, reversal of the current is presumed to be caused because the drugs absorbed in the shallow skin are released again into the gel when the electrical supply is over.

Finally, *in vivo* therapeutic effects of RIS were shown by using an osteoporosis-induced mouse model (Fig. 18). The GEL group showed almost no therapeutic effect regardless of the amount of drug loaded, which means that penetration of RIS through the skin is difficult. In the case of the $RED_{0.02}$ group, there were therapeutic effects on the mouse model almost great enough to overcome the effect of the ovariectomy.

I found that the dose-dependency is important through insufficient therapeutic effects of $RED_{0.002}$ group. I proved that the RED patch could deliver ionic drugs effectively in transdermal method by showing *in vivo* therapeutic effect.

The RED patch successfully enhanced the transdermal delivery of ionic drugs. However, transdermal drug delivery with the RED patch is required for further researches about the clinical usage. further research about the clinical usage is required for transdermal drug delivery with the RED patch. The size, and the thickness of the RED patch should be optimized for human skin for portability and flexibility. Since characteristics of drugs differ greatly, more researches should be conducted on

different types of drugs using RED patch. There should be more researches on electrical energy of the RED patch safe and acceptable for humans. Unlike commercial iontophoretic devies, the electrodeless RED patch efficiently doesn't have some disadvantages (e.g interfacial electrochemical reactions). Thus, I expect that the RED patch would allow higher maximum current densities than 0.5mA/cm^2, which is considered as upmost limitation current density for human in iontophoresis(27, 28).

5. Summary

I have developed a new and effective transdermal drug system using a miniaturized RED patch. RED patch can be activated by the salt gradient of the two solutions and be used for generating electrical energy. RED patch is biocompatible due to using drug loaded gel instead of metal electrodes. This patch is controlled by the number of ion exchange membranes in RED or the salt gradient of the solution. With *in vitro* penetration test for 3 model drugs, I confirmed that ionic drugs are effectively delivered irrespective of the charge of drugs. Then, I also checked efficient delivery and therapeutic effect of risedronate using osteoporosis induced mouse model. Therefore, the miniaturized RED patch is expected to be a promising method for drug delivery in the future.

6. Conclusion

I have conducted research to develop new drug delivery platforms with efficiency and safety. First, histidine was introduced into the LK peptide for the selective penetration into the cells at weakly acidic pH conditions around cancerous tissues. The cellular uptakes of LH peptides were promoted at the pH range from 6.5 to 6.0. The Increasing α -helicity of the LH peptide according to the pH lowering seemed to be closely related to the pH-dependent enhancement of cellular uptake. Considering the selective cell penetration activity at weakly acidic pH as well as non-cytotoxicity up to 1 μM, the LH peptide could be a promising alternative drug delivery carrier for cancer targeting in the future. Second, I developed a novel and efficient transdermal drug delivery system based on the miniaturized RED patch which can be activated by the salt gradients. RED patch can generate electric energy without any external energy source and electrodes. Furthermore, the electric potential of the RED system could be easily controlled by the salt gradients and the number of IEMs. I confirmed that the RED patch could deliver various ionic drugs into the skin in a non-invasive way. The RED patch would be an attractive transdermal delivery method for difficultly penetrable ionic drugs. I expected that these two delivery methods are promising drug delivery tools with high efficiency and safety in future pracitcal applications.

6. References

1. Stephen J., 2016 Biopharmaceutical research industry profile, RhRMA, (2016)
2. F. Jorge, Drug delivery systems: Advanced technologies potentially applicable in personalized treatments. EPMA, 1, 164-209 (2010)
3. K. Janin, Drug delivery systems—an overview. The Methods In Moelcular Biology 437, 1-50 (2008).
4. M. Lindgren, A. Prochiantz, Cell penetrating peptide, Trends in Pharmacological Sciences 21, 99-103 (2000).
5. J. Richard, Cell-penetrating peptides a reevalutation of the mechanism of cellular uptake, Journal of biological chemistry 278, 585-590 (2003).
6. M. Zorko, Cell penetrating peptides: mechanism and kinetics of cargo delivery. Advanced Drug Delivery Reviews 57, 529-545 (2005).
7. S. Jang, Cell-Penetrating, Dimeric a-Helical Peptides: Nanomolar Inhibitors of HIV-1 Transcription. Angewante Chemistry International Edition 53, 10086-10089 (2014).
8. J. Griffiths, Are cancer cells acidic? British Journal of Cancer 64, 425-427 (1991).
9. Y. Kato, Acidic extracellular microenvironment and cancer. Cancer Cell International 13, 1-8 (2013)
10. L. Fei, Tumor Targeting of a cell penetrating peptide by fusing with a pH-sensitive histidine-glutamate co-oligopeptide. Biomaterials 35, 4082-4087 (2014)
11. Z. Wang, Design of acid-activated cell penetrating peptide for deliver of active molecules into cancer cells. Bioconjugated Chemistry 22, 1410-1415 (2011)

12. M. R. Prausnitz, S. Mitragotri, R. Langer, Current status and future potential of transdermal drug delivery. Nature reviews Drug discovery 3, 115-124 (2004).

13. R. M. T. Tanner, Delivering drugs by the transdermal route: review and comment. Skin Research and Technology 14, 249-260 (2008).

14. M. R. Prausnitz, Skin barrier and transdermal drug delivery. Medical Therapy 19, 2065-2073 (2012)

15. G. K. Menon, The structure and function of the stratum corneum. International Journal of Pharmaceutics 435, 3-9 (2012)

16. P. Karande, A. Jain, S. Mitragotri, Discovery of transdermal penetration enhancers by high-throughput screening. Nature biotechnology 22, 192-197 (2004).

17. M. R. Prausnitz, Microneedles for transdermal drug delivery. Advanced Drug Delivery Reviews 56, 581-587 (2004).

18. Y. N. Kalia, A. Naik, J. Garrison, R. H. Guy, Iontophoretic drug delivery. Advanced drug delivery reviews 56, 619-658 (2004).

19. J. Michael, Pikal, The role of electroosmotic flow in transdermal iontophoresis, Advanced Drug Delivery Review 46, 281-305 (2001)

20. J. Singh, Effect of saline iontophoresis on skin barrier function and cutaneous irritation in four ethnic groups. Food and Chemical Toxicology 38, 717-726 (2000)

21. Y. N. Kalia, A. Naik, J. Garrison, R. H. Guy, Iontophoretic drug delivery. Advanced drug delivery reviews 56, 619-658 (2004).

22. A. Alexander et al., Approaches for breaking the barriers of drug permeation through transdermal drug delivery. Journal of Controlled Release 164, 26-40 (2012).

23. S. B. Tiwari, N. Udupa, Investigation into the potential of iontophoresis facilitated delivery of ketorolac. International Journal of

Pharmaceutics 260, 93-103 (2003).

24. R. A. Henry, A. Morales, C. M. Cahill, Beyond a Simple Anesthetic Effect: Lidocaine in the Diagnosis and Treatment of Interstitial Cystitis/bladder Pain Syndrome. Urology 85, 1025-1033 (2015).

25. B. Abrahamsen, Adverse effects of bisphosphonates. Calcified tissue international 86, 421-435 (2010).

26. A. M. Hounslow et al., Determination of the microscopic equilibrium dissociation constants for risedronate and its analogues reveals two distinct roles for the nitrogen atom in nitrogen-containing bisphosphonate drugs. Journal of medicinal chemistry 51, 4170-4178 (2008).

27. K. Nakamura et al., Transdermal administration of salmon calcitonin by pulse depolarization-iontophoresis in rats. International journal of pharmaceutics 218, 93-102 (2001).

28. S. Narasimha Murthy, D. E. Wiskirchen, C. Paul Bowers, Iontophoretic drug delivery across human nail. Journal of pharmaceutical sciences 96, 305-311 (2007).

7. Figures

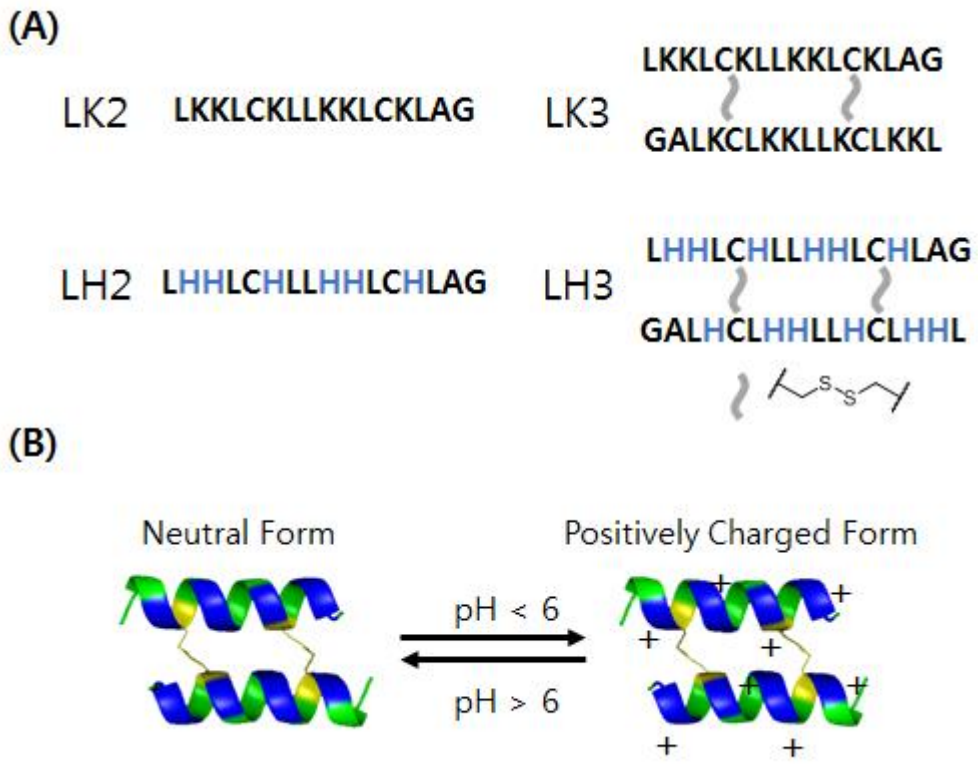

Fig. 1. The sequence of LK (LK2, monomer/ LK3, dimer) and LH peptides (LH2, monomer/ LH3, dimer) (A) and charge change of LH3 according to pH (B)

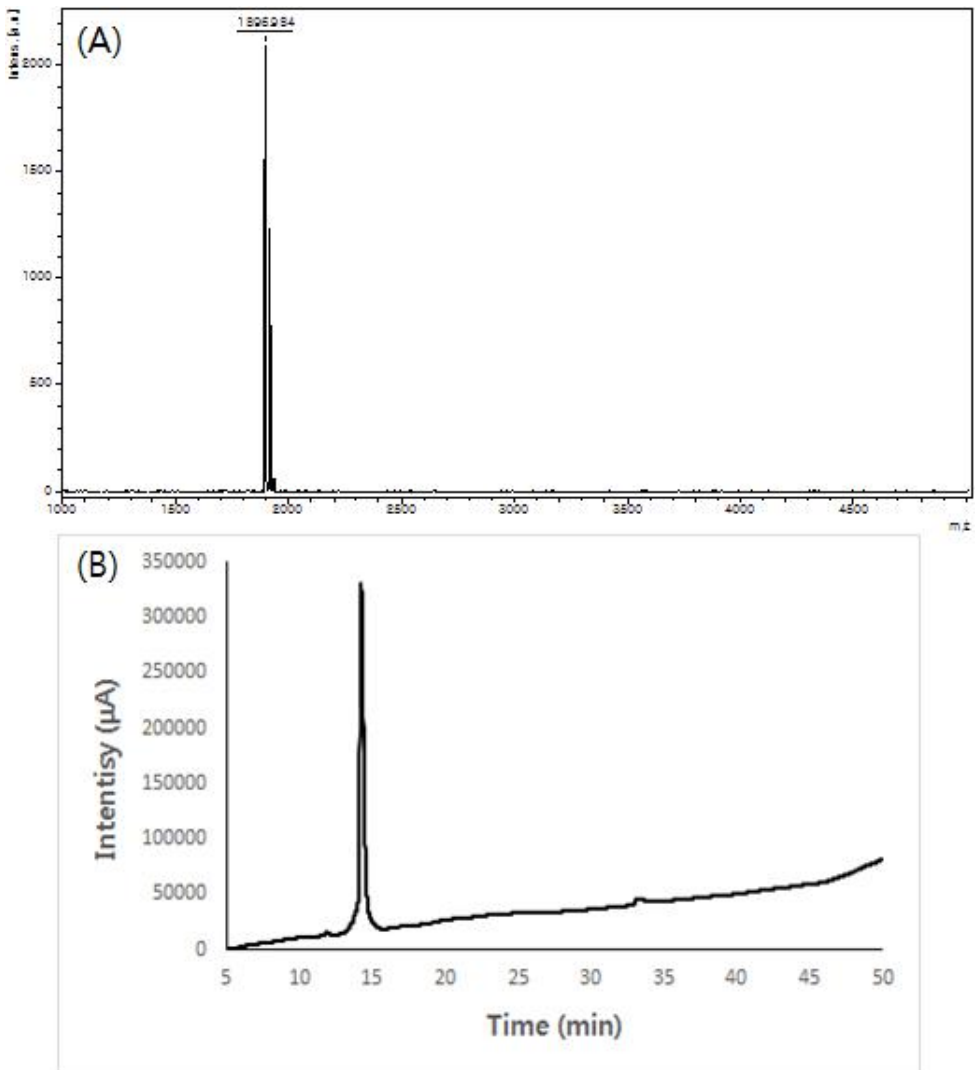

Fig. 2. The results of MALDI - TOF (A) and HPLC analysis (B) of N-terminus acetylated LH2.

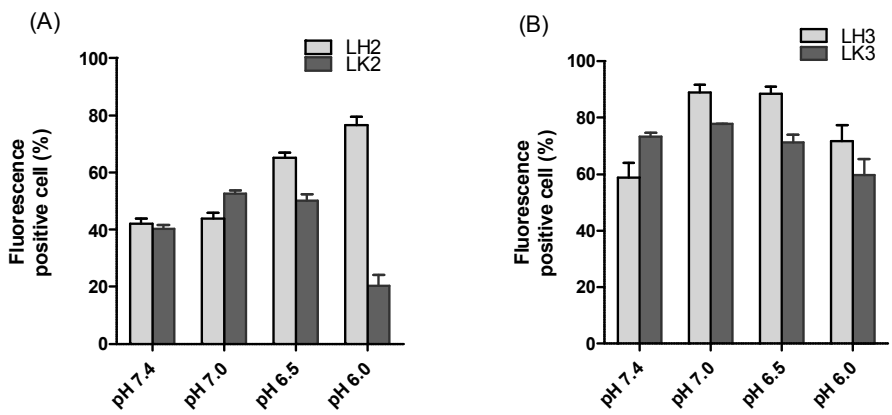

Fig. 3. *In vitro* cellular uptake of LK, LH peptides. (A) 100nM LH, LK monomers were treated with MDA-MB-231 cells for 4 hours at 37°C. (B) 25nM LH, LK dimers were treated with MDA-MB-231 cells for 4 hours at 37°C.

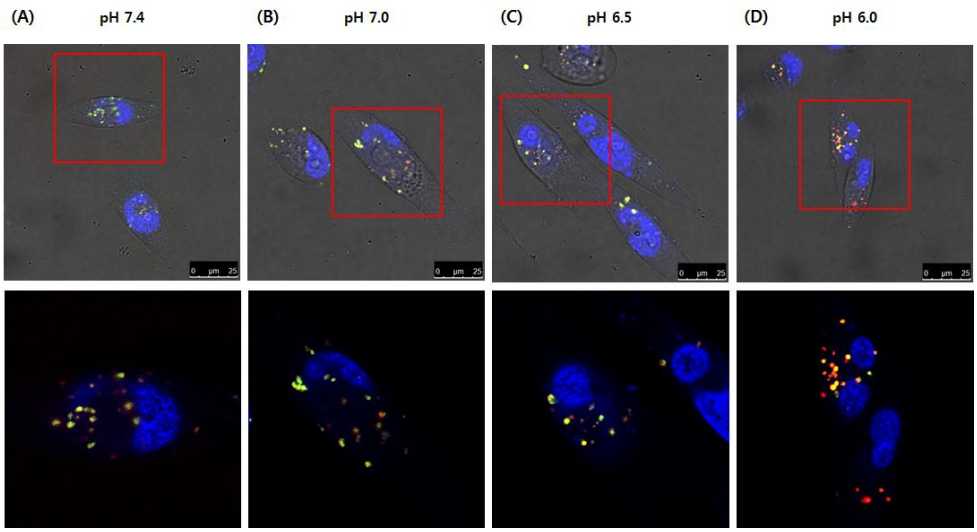

Fig. 4. Confocal laser scanning microscopy (CLSM) images of MDA-MB-231 cells. Rhodamine-labeled LH3 (25nM, red) was treated to MDA-MB-231 cells at four pH conditions for 16 hours (A: pH 7.4, B: 7.0, C: 6.5 and D: 6.0). Nuclei and lysosomes were stained with Hoechst 33342 (blue) and Lysotracker (green), respectively.

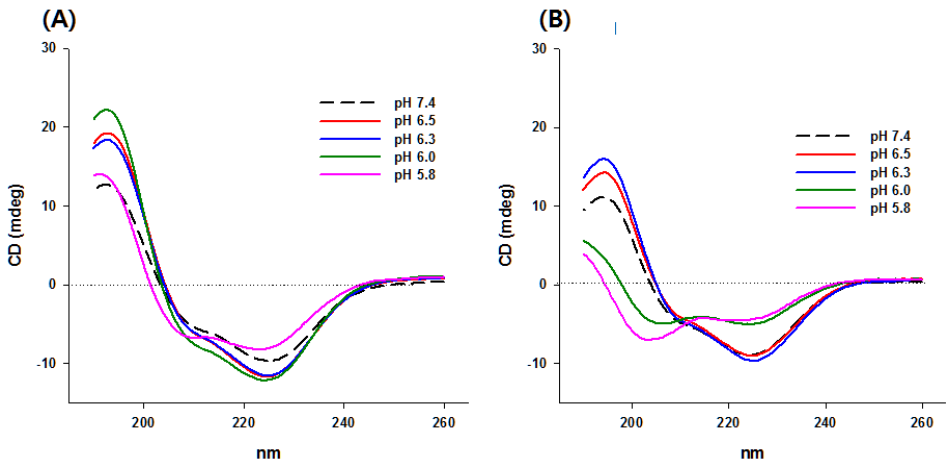

Fig 5. CD spectra of 10μM LH2 in 10mM phosphate buffer (A) and 10μM LK2 in 10mM phosphate buffer.

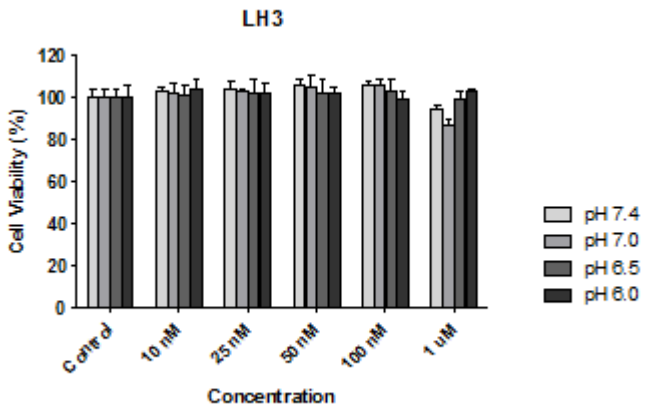

Fig. 6. Cytotoxicity of LH dimer(LH3) against MDA-MB-231 cells for 4 hours at different pH and concentration conditions.

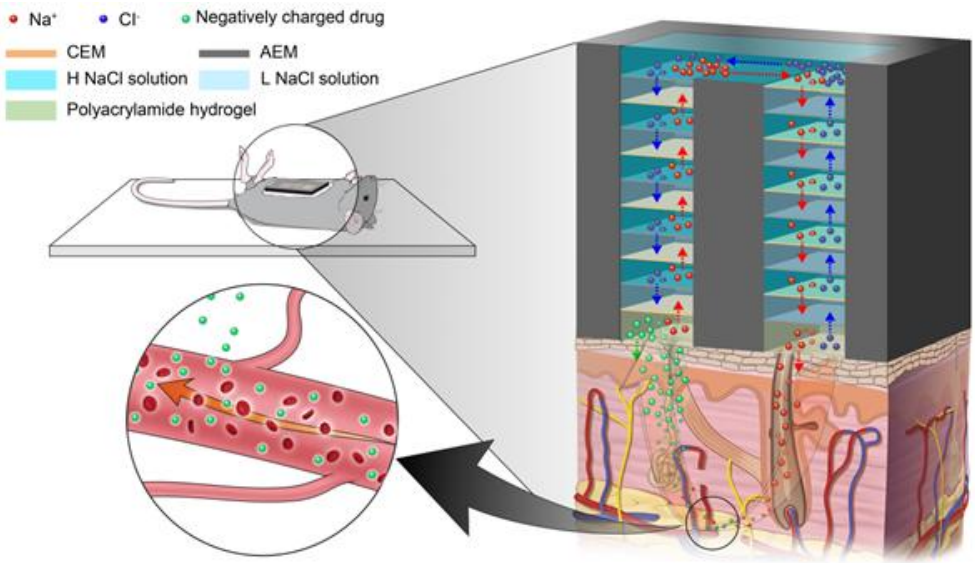

Fig. 7. A new type of transdermal drug delivery driven by the salt gradient via RED system. Schematic representation of the RED patch attached on the mouse skin. Na^+ and Cl^- in the RED system move from the high concentrated (H) NaCl solution to low concentrated (L) solution through ionexchage membranes.

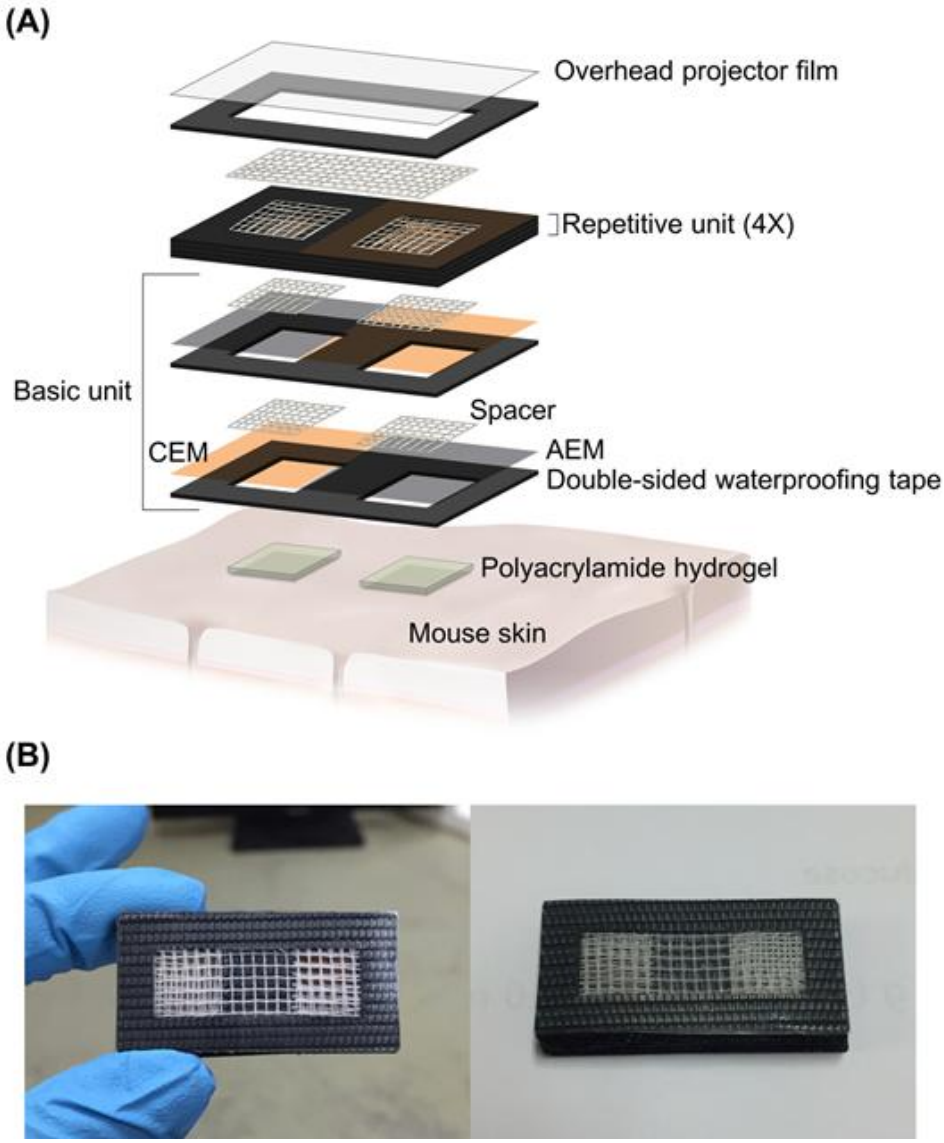

Fig. 8. The structure of the miniaturized RED patch. (A) three-dimensional image of RED patch showing components in detail. (B) Real images of an RED patch.

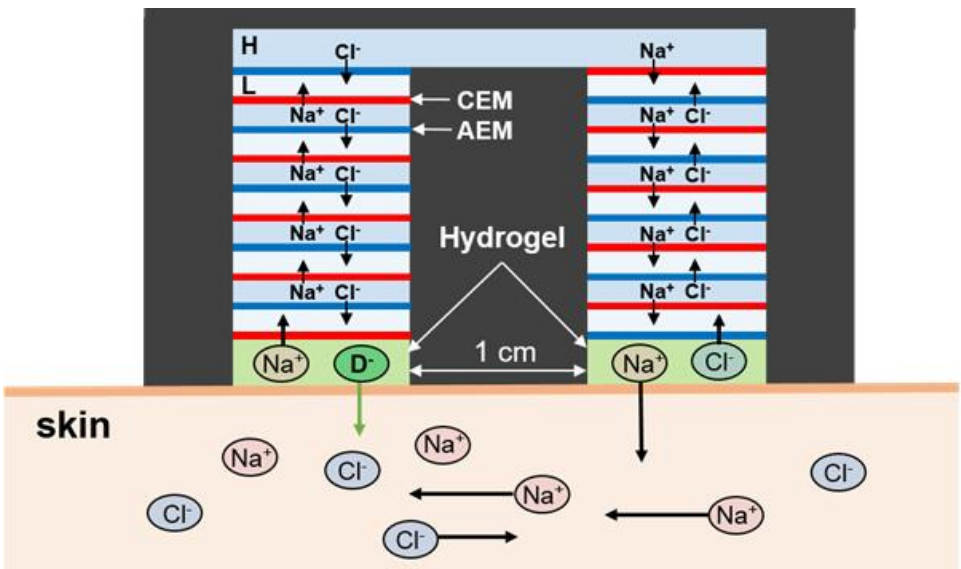

Fig. 7. Schematic representation of the miniaturized RED patch consisting of 10 pair of ion-exchange membranes (IEMs). All spaces between the IEMs is 500 μm thick except for the top floor (750 μm). The hydrogel storing drugs (left side) is pressed by negative potential compared to hydrogel containing 50 mM NaCl (right side). In case of positively charged drugs, it should be in the right hydrogel while the other hydrogel contains only NaCl salt. (H, high concentrated NaCl solution; L, low-concentrate NaCl solution; CEM, cation-exchange membrane; AEM, anion-exchange membrane.)

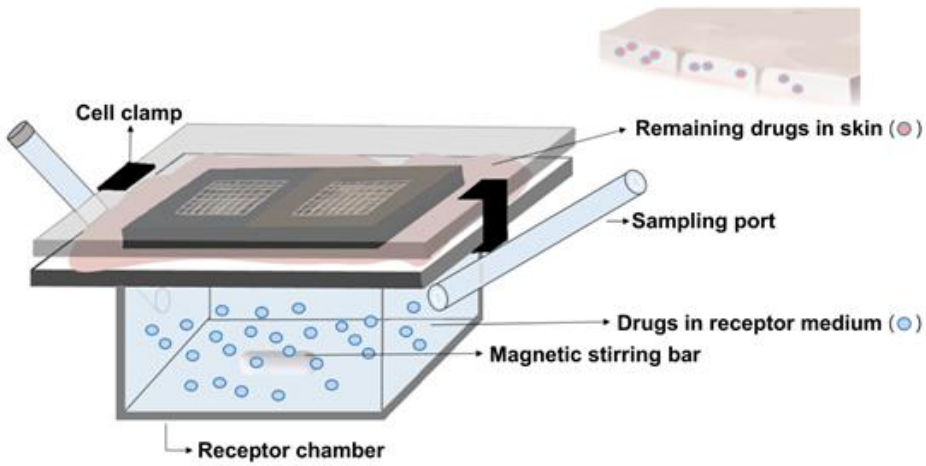

Fig. 8. Schematic images of the modified Franz diffusion cell for *in vitro* test using the RED patch. The Franz cell were sustained under a constant condition (37 ℃ , 200 rpm stirring). The residual amount of drug in the skin and the penetrated amount of drug through the skin were measured over administration of drug.

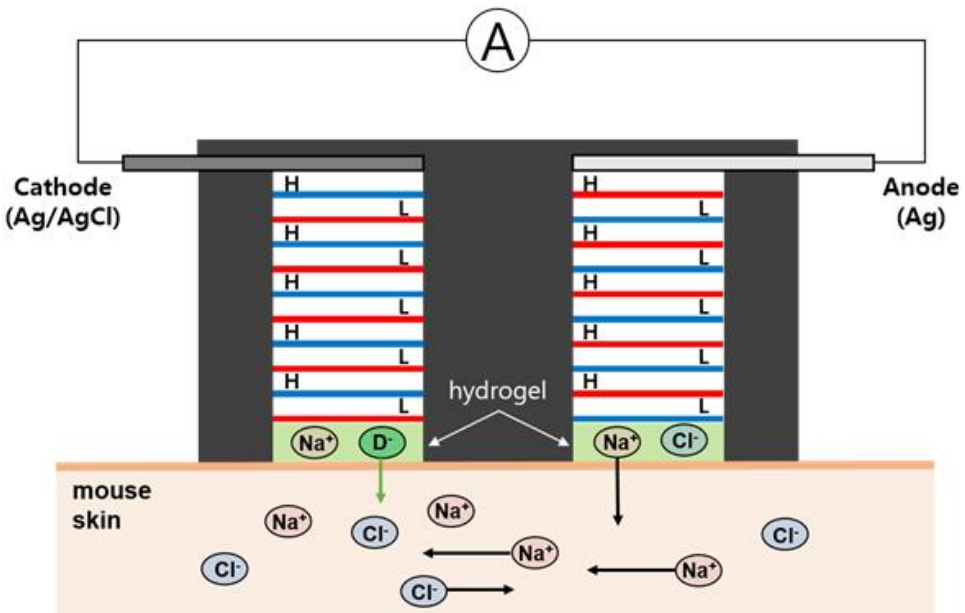

Fig. 11. The schematic image of RED patch with the electrodes to measure the current during *in vitro* and *in vivo* penetration tests.

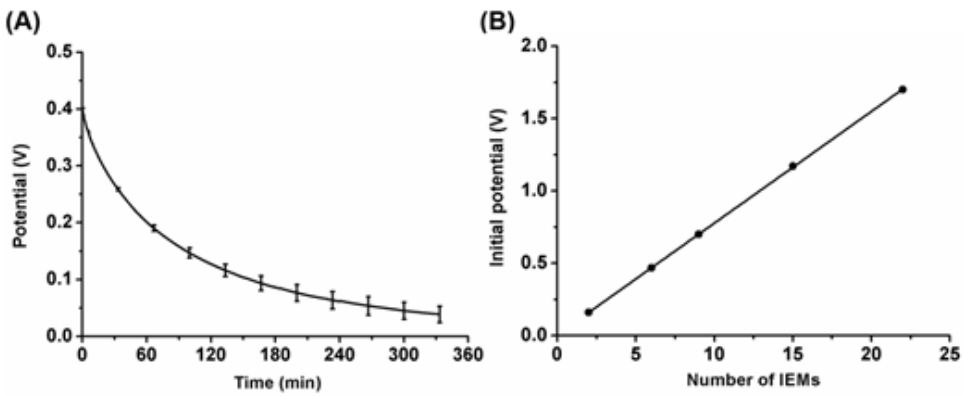

Fig. 12. Electrical properties of the miniaturized RED patches. Potential changes of RED patches with 9.79 kΩ external resistor (A). Initial potentials obtained after injection of NaCl solutions (0.017 and 0.51 M NaCl) alternatively over the number of IEMs used in the RED (B).

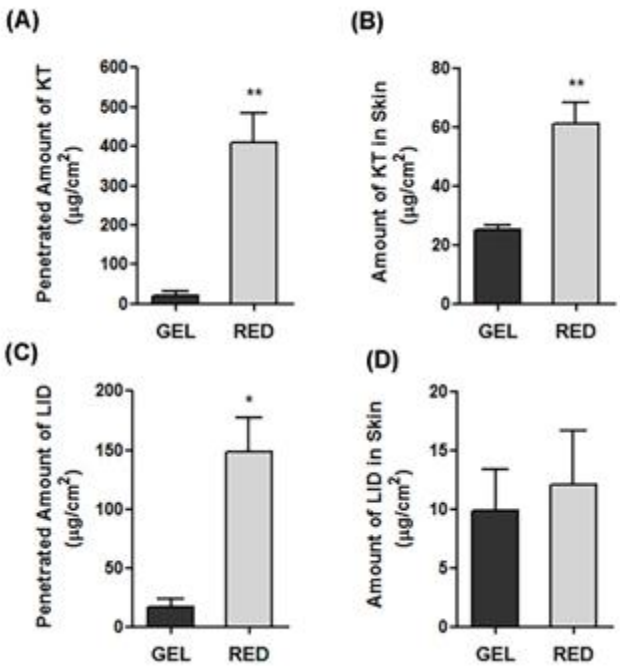

Fig. 13. *In vitro* penetration test of KT and LID. The comparison of drug amounts between GEL and RED patch through the freshly prepared mouse skin. The graphs representing the amount of KT that penetrated through the skin (A), the residual amount of KT in skin (B), the amount of LID that penetrated through the skin (C), and the residual amount of LID in skin (D). All drugs were incorporated to the polyacrylamide hydrogel matrix with 2% (w/v, 3 mg per patch) concentration. * $P < 0.05$, ** $P < 0.005$.

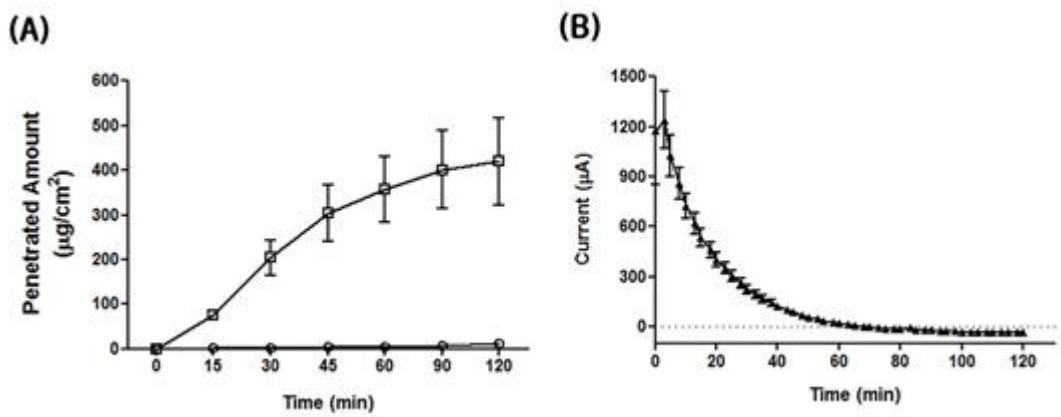

Fig. 14. *In vitro* penetration test of 2% RIS (w/v) using GEL (○) and RED patch (□). The graphs represent the cumulative amount of RIS with the administration time (A) and the current response of the RED patch during *in vitro* penetration test (B).

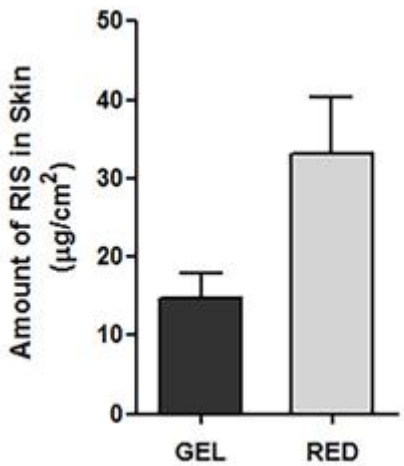

Fig. 15. *In vitro* penetration test: the graph presents the RIS amounts in the skin layers after 2 h since REDs and GELs were attached.

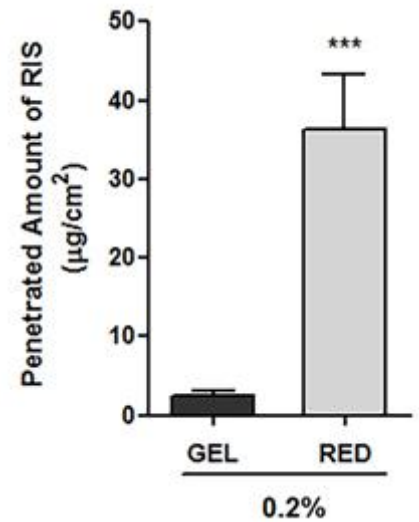

Fig. 16. *In vitro* penetration test of RIS with 0.2% concentration for GEL and RED patches. Graphs show the total amounts of RIS penetrated through the mouse skin for 2 h. *** $P < 0.0005$.

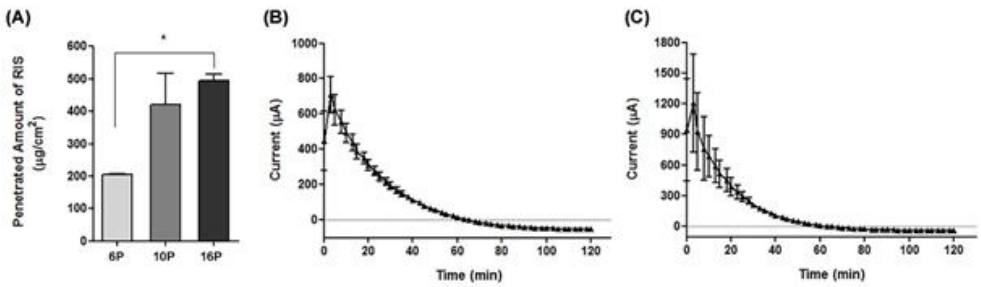

Fig. 17. *In vitro* penetration test of RIS in RED_{6P} and RED_{16P}. The graphs show the penetrated amounts of RIS (A), the current change in RED6P (B) and RED16P (C).

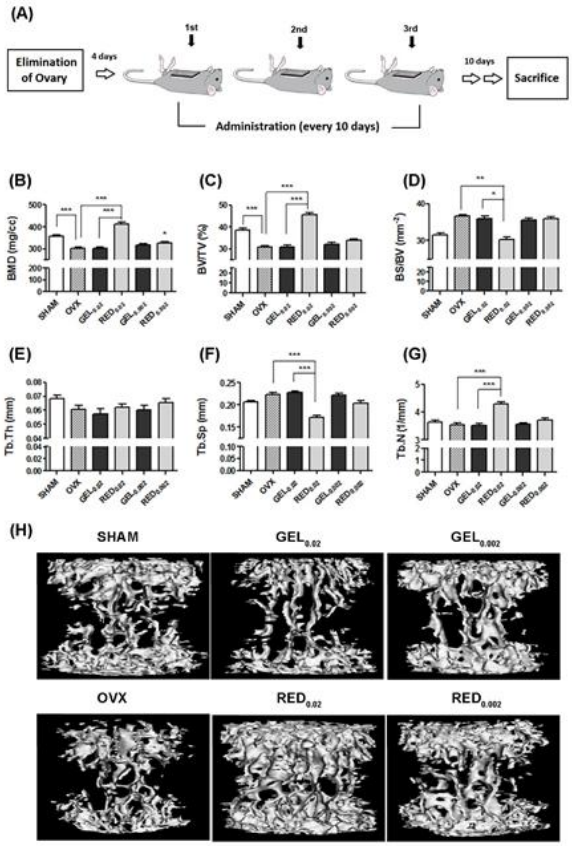

Fig. 18. Therapeutic effects of RIS on osteoporosis induced mouse model using RED and GEL. (A) Schema of experiments, (B) Bone mineral density (BMD), (C) bone volume per total volume (BV/TV), (D) bone surface (BS/BV), (E) trabecular thickness (Tb.Th), (F) trabecular separation (Tb.Sp), (G) trabecular number (Tb.N), and (H) the representative images of the vertebrae of the ovariectomized mouse. *P < 0.05, **P < 0.005, ***P < 0.0005.

Number of IEMs	6 pairs (RED_{6p})	10 pairs (RED)	16 pairs (RED_{16p})
Initial Volatage (V)	1.34 ± 0.04	2.23 ± 0.14	3.45 ± 0.29

Table 2. Voltage from REDs with various number of IEM pairs.

국문 초록

본 연구의 목적은 생물학적 시스템에서 약물의 효능과 안전성을 높이는 것이다. 연구에는 두 가지 방법이 사용되었다.

첫 번째 연구는 류신과 라이신으로 구성되어 10 nM 수준에서 높은 세포 투과성을 가지는 세포 투과성 펩타이드인, LK 펩타이드에 pH 선택성을 부여하는 것이다. LK 펩타이드의 서열에 pKa가 6.0인 히스티딘을 도입하여 펩타이드에 pH 감응성을 띄도록 하였다. 그 결과, 약 pH 6에서 양성자화되어 세포 내 투과 시, 양전하를 띄는 새로운 LH 펩타이드를 개발했다. 암 조직 주변의 pH가 약 5-6이기 때문에 LH 펩타이드는 암-표적 약물 전달체로 사용될 수 있다. LH 펩타이드가 pH에 따라 선택적으로 세포 내로 침투한다는 것을 확인했다. 또한, 여러 pH 조건에서 LH 펩타이드의 독성을 비교했다.

두 번째 연구로, 경피 투과성 약물 전달 시스템에 연전기투석 기술을 도입했다. RED 패치는 서로 다른 농도를 가지는 두 용액이 이온 선택성 막들을 통과하여 형성되는 이온 구배를 통해 전기 에너지를 생성할 수 있다. 이온성 약물을 피부에 전달하기 위해 역전기투석으로부터 생성된 전기 에너지를 사용했다. *In vitro* 투과 시험에서는 역전기투석 시스템을 통해 이온 약물이 효율적으로 전달되었음을 확인했다. 마지막으로, 협동 연구를 통해 골다공증 유발 마우스 모델에서 RED가 전달한 리세드로네이트의 생체 내 약리 효과를 조사했다.

나는 두 연구가 앞으로 높은 효율과 안전성을 가지는, 약물 전달을 위한 효과적인 대안으로 사용될 것으로 기대한다.

주요어: pH-선택성, 세포투과성 펩타이드, 역전기투석(RED), 경피 약물 전달 시스템, 리제드로네이트, 이온도입법, 골다공증, 리제드로네이트

학번: 2015-20402